Optimization of the split-spectrum amplitude-decorrelation angiography algorithm on a spectral optical coherence tomography system

Simon S. Gao, Gangjun Liu, David Huang, and Yali Jia*

Casey Eye Institute, 3375 SW Terwilliger Blvd., Portland, Oregon 97239, USA
**Corresponding author: jiaya@ohsu.edu*

Received February 23, 2015; revised April 21, 2015; accepted April 22, 2015;
posted April 23, 2015 (Doc. ID 235085); published May 8, 2015

The split-spectrum amplitude-decorrelation angiography algorithm was optimized on a spectral optical coherence tomography system using a flow phantom. The number of times the spectrum was split and the bandwidth of each split were adjusted to maximize the flow phantom decorrelation signal-to-noise ratio. The improvement in flow detection was then demonstrated with en face retinal angiograms. The optimized algorithm increased the detectable retinal microvascular flow and decreased the variability of the quantified vessel density in OCT retinal angiograms of healthy human subjects. © 2015 Optical Society of America

OCIS codes: (110.4500) Optical coherence tomography; (170.3880) Medical and biological imaging.
http://dx.doi.org/10.1364/OL.40.002305

Optical coherence tomography (OCT) is a noninvasive, interferometric imaging modality that has a variety of applications. In particular, a number of algorithms and/or techniques using OCT have been developed for vascular imaging in the eye. A set of these methods rely on Doppler OCT [1], which assesses blood flow by comparing phase differences between adjacent A-scans. While effective for quantifying flow in larger blood vessels [2], Doppler OCT is insensitive to transverse flow and is not efficient at detecting the slower flow within the microvasculature of the retina [3,4]. Other methods such as optical micro-angiography [5] and speckle variance OCT [6,7] have been developed to visualize microcirculation. Previously, we presented an improvement on the speckle variance method called split-spectrum amplitude-decorrelation angiography (SSADA). The algorithm was implemented on a custom-built swept-source OCT system [8], and it was shown to be able to identify reduced flow in the optic disk in glaucoma patients [9] and choroidal neovascularization in age-related macular degeneration patients [10]. To allow for wider adoption of the technique, we sought to implement and optimize the SSADA algorithm on a spectrometer-based (spectral) OCT system, as most commercial OCT retinal scanners are spectral OCT systems. Herein, we show how the algorithm was optimized using a flow phantom to maximize the decorrelation signal-to-noise ratio (DSNR) and the subsequent improvement in flow detection in *en face* retinal angiograms.

A 0.1% Intralipid flow phantom was scanned using a commercial, spectral OCT system (RTVue-XR, Optovue, CA) with a center wavelength of 840 nm, full width at half maximum (FWHM) bandwidth of 45 nm, axial resolution of 5 μm in tissue, collimated spot diameter of 1.1-mm full width at $1/e^2$, which results in an estimated airy disk beam spot size on the retina of 22 μm, and A-scan rate of 70 kHz. An achromatic doublet (AC254-030-B, Thorlabs Inc., New Jersey) was used to focus the light on to the flow channel. The plastic channel had an inner diameter of 0.5 mm. A syringe pump (11 Plus, Harvard Apparatus, Massachusetts) was used to generate an average flow velocity of approximately 1.7 mm/s within the channel. The Intralipid concentration was chosen because it provided uniform signal intensity in the 0.5-mm depth range. Two sequential B-scans each consisting of 304 A-scans were taken at the same location to detect flow with the SSADA algorithm. The theory and details of the algorithm have previously been reported [8]. Briefly, the raw interferogram, or full spectrum, was split via Gaussian filters into a set of spectral splits. The center positions of the filters were evenly spaced across the regions of the interferogram which had a spectral envelope amplitude greater than −12 dB. The FWHM bandwidth of the filters was set such that all of the original signal was used in the processing. The OCT reflectance image of each spectral split was then generated as the amplitude of the Fourier transform of the spectrum. The decorrelation of each pixel in the x (transverse) and z (axial) directions between the sequential OCT reflectance images was then calculated as

$$\bar{D}(x,z) = 1 - \frac{1}{M}\sum_{m=1}^{M} \frac{A_{1,m}(x,z)A_{2,m}(x,z)}{\left[\frac{1}{2}A_{1,m}(x,z)^2 + \frac{1}{2}A_{2,m}(x,z)^2\right]}, \quad (1)$$

where M is the number of spectral splits; each split is denoted by subscript m; $A_{1,m}$ and $A_{2,m}$ are the reflectance amplitudes of the mth spectral split from the two sequential cross-sectional OCT scans. The DSNR of the flow phantom (DSNR_phantom) was defined as the mean of the decorrelation within the flow channel divided by the standard deviation of the decorrelation in a nearby static region. The static material was paper, and the noise region was chosen such that it did not include the paper surface.

The log OCT reflectance and decorrelation images of the flow phantom are shown in Figs. 1(A) and 1(B), respectively. By adjusting the number of times the spectral interferogram was split and the FWHM bandwidth of each split in the SSADA algorithm, we generated a set of decorrelation images. The DSNR_phantom was calculated for each decorrelation image, and Fig. 1(C) shows the relationship between the number of spectral splits,

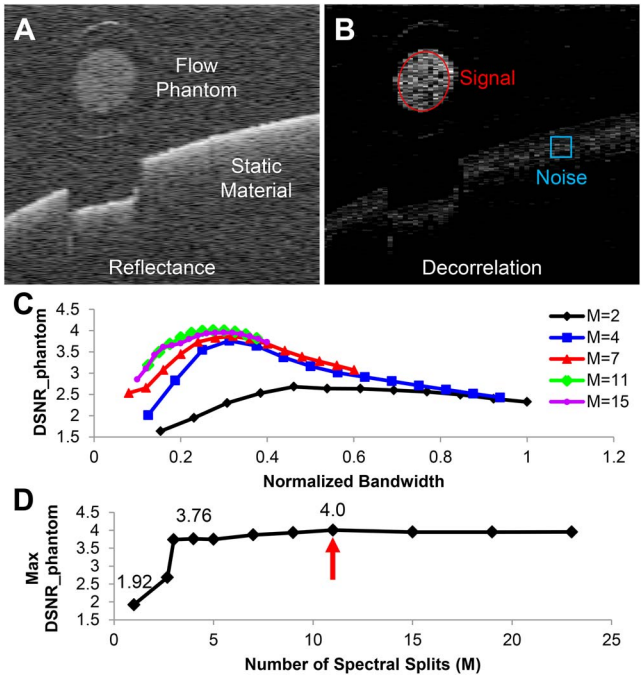

Fig. 1. (A) Log OCT reflectance image of the flow phantom. (B) Decorrelation image calculated from two sequential B-scan images at the same location. The circled signal and boxed noise regions were used to calculate the DSNR of the decorrelation image (DSNR_phantom). (C) Plot depicting the relationship between the number of spectral splits (M), normalized bandwidth to the system spectral bandwidth, and DSNR_phantom. (D) Plot of the maximum DSNR_phantom for a given M. The corresponding normalized bandwidths are 1, 0.46 for $M = 2$, 0.27 for $M = 3$, 0.31 for $M = 4$, 0.35 for $M = 5$, 0.32 for $M = 7$, 0.33 for $M = 9$, 0.28 for $M = 11$, 0.30 for $M = 15$, 0.27 for $M = 19$, and 0.27 for $M = 23$. The numerical DSNR_phantom values for $M = 1$, 4, and 11 are shown. M of one represents the use of the full spectrum. The red arrow shows that the highest DSNR_phantom was achieved when $M = 11$.

normalized bandwidth to the system spectral bandwidth, and DSNR_phantom. For a given number of spectral splits, there is local maximum DSNR_phantom. In a previous study utilizing split-spectrum Doppler OCT, Vuong *et al.* observed a similar effect where there was a local minimum of the phase noise as the normalized bandwidth of the spectral split was adjusted [11]. By plotting the maximum DSNR_phantom for a given number of spectral splits irrespective of the normalized bandwidth, we see in Fig. 1(D) that 11 spectral splits ($M = 11$) resulted in the highest DSNR_phantom value. The corresponding spectral split bandwidth was 12.4 nm, with a normalized bandwidth value of 0.28. Increasing M beyond 11 did not improve the SNR. Further investigation revealed that the spectral split covering the extremes of the full spectrum added little information and when averaged would serve to slightly reduce the SNR. For example, not including the first and last spectral split for $M = 15$ improved the DNSR_phantom by 2.3%. Increasing M also increased the amount of computation time required to produce relevant images. This was particularly apparent when dealing with volumetric data, although implementing the data processing on a graphics processing unit or field-programmable gate array would reduce computation time.

We then determined the improvement in flow detection *in vivo* using the newly derived parameters of 11 spectral splits ($M = 11$) each with a normalized bandwidth of 0.28 over simply using the full spectrum ($M = 1$) or the originally reported 4 spectral splits ($M = 4$) each with a normalized bandwidth of 0.39. The human study protocol was approved by the Oregon Heath & Science University Institutional Review Board and followed the tenets of the Declaration of Helsinki in the treatment of human subjects. Five healthy subjects (age 35.6 ± 9.7 years) were imaged using the same commercial, spectral OCT system that was used for the flow phantom experiment. The imaging protocol consisted of two volumetric scans covering a 3×3 mm scanning area centered on either the fovea or optic disk. For each volumetric scan, in the fast transverse scanning direction, 304 A-scans were sampled to obtain a single B-scan. Two sequential B-scans were collected at each location for flow detection. In the slow transverse scanning direction, 304 locations were sampled. The fast scanning direction was in the horizontal direction (x-fast) for one volume and in the vertical direction (y-fast) for the other.

For each volume, the OCT structural B-scan images were processed using the full spectrum. Three sets of decorrelation images were generated using the full spectrum, originally reported SSADA algorithm parameters, and newly determined SSADA algorithm parameters from the flow phantom experiment. While the SSADA algorithm reduces the effect of noise resulting from bulk axial motion by degrading the axial resolution, additional compensation for bulk motion was performed by subtracting the median decorrelation value for each average decorrelation B-scan frame. Motion artifacts were further minimized by 3D orthogonal registration based on the structural information and merging of x-fast and y-fast volumes [12]. An automated algorithm identified the inner limiting membrane (ILM) and retinal pigment epithelium (RPE) [13]. The *en face* macular angiogram was then generated as the maximal projection of the decorrelation value between the ILM and RPE.

Figures 2(A) and 2(B) show representative macular angiograms processed using the SSADA algorithm when $M = 4$ and 11, respectively. These images have a minimum threshold determined from the mean plus two standard deviations of the decorrelation values within their foveal avascular zone (FAZ). To quantify the improvement, we calculated the macular angiogram DSNR (DSNR_retina) from the original angiograms as

$$\text{DSNR\_retina} = \frac{\bar{D}_{\text{Parafovea}} - \bar{D}_{\text{FAZ}}}{\sqrt{\sigma^2_{\text{FAZ}}}}, \tag{2}$$

where $\bar{D}_{\text{Parafovea}}$ and $\bar{D}_{\text{FAZ}}$ are the average decorrelation values within the parafoveal annulus shown in green and FAZ shown in white in Fig 2(A), respectively, and σ^2_{FAZ} is the variance of the decorrelation within the FAZ. The radii of the white and green circles are 0.3, 0.65, and 1 mm. Figure 2(C) shows the increase in average DSNR_retina from the five subjects as the number of spectral splits in the SSADA processing was increased from $M = 1$ to 4 to 11.

Clinically, DSNR_retina does not confer useful information beyond the quality of the angiogram. Instead, the

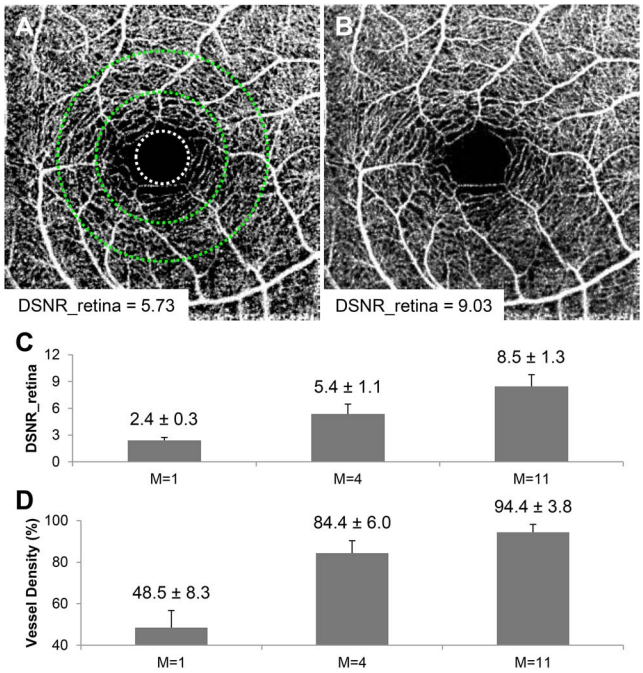

Fig. 2. (A) *En face* macular angiogram processed using the SSADA algorithm when $M = 4$. DSNR_retina was calculated between the parafoveal annulus in green and the FAZ in white. (B) Angiogram processed using the SSADA algorithm when $M = 11$. (C) DSNR_retina for angiograms from five healthy subjects processed using the SSADA algorithm when $M = 1$, the originally reported SSADA algorithm parameters ($M = 4$, normalized spectral split bandwidth of 0.39), and the newly determined SSADA algorithm parameters ($M = 11$, normalized bandwidth of 0.28). Data are presented as mean ± standard deviation. (D) The vessel density value of the angiograms processed under the same conditions.

vessel density of the parafoveal region can be assessed. This is often qualitatively judged using fluorescein angiography when trying to identify regions of capillary dropout in patients with diseases such as diabetic retinopathy. The vessel density metric has previously been shown to be able to identify reduced flow in the optic nerve head in glaucoma patients [9]. Parafoveal vessel density was defined as the percentage of the area within the outermost green circle shown in Fig. 2(A), excluding the FAZ, that had detectable flow. The threshold for detecting flow was set at two standard deviations above the mean decorrelation signal within the FAZ. Figure 2(D) shows the increase in average vessel density from 5 healthy subjects as the number of spectral splits in the SSADA processing was increased. Furthermore, we observed a decrease in the standard deviation of the measured vessel density as M was increased in the SSADA processing. The optic disk was also scanned in these subjects. Figures 3(A) and 3(B) show representative optic disk angiograms processed using the SSADA algorithm when $M = 1$ and 11, respectively.

To summarize, we optimized the SSADA algorithm using a flow phantom to maximize DSNR and demonstrated the improvement in flow detection in *en face* retinal angiograms. In the initial Letter, the SSADA algorithm was implemented on a swept-source OCT system. Using the SSADA algorithm with $M = 4$ and eight sequential

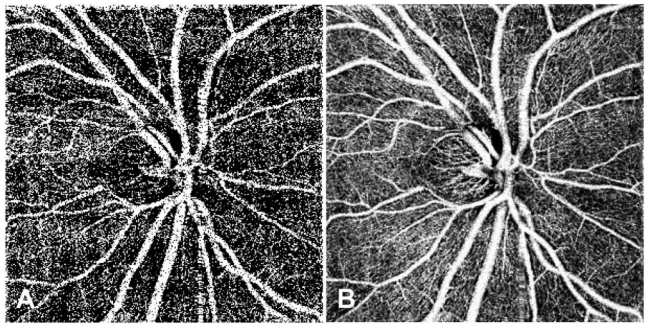

Fig. 3. (A) *En face* optic disk angiogram processed using the SSADA algorithm when $M = 1$. (B) Angiogram processed using the SSADA algorithm when $M = 11$.

B-scans at the same location, DSNR_retina approximately doubled compared to using the full spectrum. A comparable increase was observed using the 70-kHz spectral OCT system despite only using two sequential scans at the same location. After optimization and using SSADA with $M = 11$ each with a normalized bandwidth of 0.28, DSNR_retina increased by an additional factor of 1.57 when compared to $M = 4$. DSNR_phantom, in comparison, increased by a factor of 1.06 from $M = 4$ to 11. The greater improvement in DSNR_retina is likely associated with the *en face* image being composed of information from multiple B-scans. This implementation of the SSADA algorithm likewise degraded the axial resolution to approximately 18 μm in tissue, which was deemed acceptable as the *en face* presentation of angiograms required a depth projection. Sacrificing some of the DSNR improvement by using a larger spectral split bandwidth to preserve the axial resolution might be a worthwhile tradeoff in cases such as the investigation of flow in the thin choriocapillaris layer. Nevertheless, the increased ability to detect microvascular flow, as indicated by the increase in vessel density, coupled with the decreased variability in detecting flow, as indicated by the reduced vessel density standard deviation, will add to the clinical utility of SSADA based OCT angiography.

The authors gratefully acknowledge Rahul Chandwani and Varun Gopinatth for technical assistance and study coordinators Janice Ladwig and Denzil Romfh for scanning the subjects. This work was supported by NIH grants R01 EY023285, R01 EY024544, DP3 DK104397, T32 EY23211; CTSA grant UL1TR000128; and an unrestricted grant from Research to Prevent Blindness.

References

1. J. A. Izatt, M. D. Kulkarni, S. Yazdanfar, J. K. Barton, and A. J. Welch, Opt. Lett. **22**, 1439 (1997).
2. B. White, M. Pierce, N. Nassif, B. Cense, B. Park, G. Tearney, B. Bouma, T. Chen, and J. de Boer, Opt. Express **11**, 3490 (2003).
3. R. K. Wang and Z. Ma, Opt. Lett. **31**, 3001 (2006).
4. R. K. Wang and L. An, Opt. Express **17**, 8926 (2009).
5. L. An and R. K. Wang, Opt. Express **16**, 11438 (2008).
6. A. Mariampillai, M. K. Leung, M. Jarvi, B. A. Standish, K. Lee, B. C. Wilson, A. Vitkin, and V. X. Yang, Opt. Lett. **35**, 1257 (2010).
7. A. Mariampillai, B. A. Standish, E. H. Moriyama, M. Khurana, N. R. Munce, M. K. Leung, J. Jiang, A. Cable,

B. C. Wilson, I. A. Vitkin, and V. X. Yang, Opt. Lett. **33**, 1530 (2008).
8. Y. Jia, O. Tan, J. Tokayer, B. Potsaid, Y. Wang, J. J. Liu, M. F. Kraus, H. Subhash, J. G. Fujimoto, J. Hornegger, and D. Huang, Opt. Express **20**, 4710 (2012).
9. Y. Jia, J. C. Morrison, J. Tokayer, O. Tan, L. Lombardi, B. Baumann, C. D. Lu, W. Choi, J. G. Fujimoto, and D. Huang, Biomed. Opt. Express **3**, 3127 (2012).
10. Y. Jia, S. T. Bailey, D. J. Wilson, O. Tan, M. L. Klein, C. J. Flaxel, B. Potsaid, J. J. Liu, C. D. Lu, M. F. Kraus, J. G. Fujimoto, and D. Huang, Ophthalmology **121**, 1435 (2014).
11. B. Vuong, A. M. Lee, T. W. Luk, C. Sun, S. Lam, P. Lane, and V. X. Yang, Opt. Express **22**, 7399 (2014).
12. M. F. Kraus, B. Potsaid, M. A. Mayer, R. Bock, B. Baumann, J. J. Liu, J. Hornegger, and J. G. Fujimoto, Biomed. Opt. Express **3**, 1182 (2012).
13. O. Tan, G. Li, A. T. Lu, R. Varma, and D. Huang, Ophthalmology **115**, 949 (2008).